CrossMark

Multiplex Inertio-Magnetic Fractionation (MIMF) of magnetic and non-magnetic microparticles in a microfluidic device

Vikash Kumar[1] · Pouya Rezai[1]

Abstract Separation of multiple microparticles at high throughput is highly required in different applications such as diagnostics and immunomagnetic detection. We present a microfluidic device for multiplex (i.e., duplex to fourplex) fractionation of magnetic and non-magnetic microparticles using a novel hybrid technique based on interactions between flow-induced inertial forces and countering magnetic forces in a simple expansion microchannel with a side permanent magnet. Separation of more than two types of particles solely by inertia or magnetic forces in a straight microchannel is challenging due to the inherent limitations of each technique. By combining inertial and magnetic forces in a straight microchannel and addition of a downstream expansion hydrodynamic separator, we overcame these limitations and achieved duplex to fourplex fractionation of magnetic and non-magnetic microparticles with high throughput and efficiency. Particle fractionation performance in our device was first optimized with respect to parameters such as flow rate and aspect ratio of the channel to attain coexistence of inertial and magnetic focusing of particles. Using this scheme, we achieved duplex fractionation of particles at high throughput of 10^9 particles per hour. Further, we conducted experiments with three magnetic particles (5, 11 and 35 µm) to establish their size-dependent ordering in the device under combined effects of magnetic and inertial forces. We then used the findings for fourplex fractionation of 5, 11 and 35 µm magnetic particles from non-magnetic particles of various sizes (10–19 µm). This Multiplex Inertio-Magnetic Fractionation (MIMF) technique offers a simple tool to handle complex and heterogeneous samples and can be used for affinity-based immunomagnetic separation of multiple biological substances in fluidic specimens in the future.

1 Introduction

Separation of small substances such as micro- and nanoparticles, amino acids and cells distinctly from a heterogeneous sample is critical for many applications such as cellomics (Andersson and van den Berg 2003), genomics (Yilmaz and Singh 2012), diagnosis (Saliba et al. 2010; Ozkumur et al. 2013) and immunoassays (Lim and Zhang 2007). Fluorescence-activated cell sorting (FACS) (Julius et al. 1972) is one of the most commonly used methods for sorting targets based on their fluorophore labeling. But FACS needs compatibility of targets with fluorescent tagging and requires in-line fluorescent imaging, analysis and downstream sorting that makes the technique complex, expensive and inaccessible. Several microfluidic-based methods such as deterministic lateral displacement (DLD) (Huang et al. 2004), pinched flow fractionation (PFF) (Yamada et al. 2004) and spiral microfluidics (Bhagat et al. 2010) have been developed to execute multi-particle sorting. DLD method works at low throughput and its performance is marred by the frequent clogging of particles in the device. PFF also works at very low throughput and cannot be operated without a diluting sheath flow. Spiral microfluidic devices can be used for multiplex sorting [e.g., fourplex sorting in (Sarkar et al. 2016)], but the technique still

✉ Pouya Rezai
 prezai@yorku.ca

1   Department of Mechanical Engineering, York University,
     BRG 433B, 4700 Keele St, Toronto, ON M3J 1P3, Canada

requires a high ratio of sample to sheath flow and its operation is highly constrained by the geometry of the channel and limited to a narrow range of flow rates. Moreover, DLD, PFF and spiral microfluidic sorting methods have a common limitation of sorting particles based on the difference in their sizes which means that sorting of two particles with identical or very close sizes, but different inherent characteristics such as magnetization cannot be achieved with these methods.

To address the limitations above, the magnetophoretic separation technique has received a significant attention. Magnetic sorting has unique operational advantages as it is reasonably unperturbed by changes in medium temperature or particle characteristics such as surface charge and ionic concentration (Zhu et al. 2014). Miltenyi et al. (1990) used macroscale chromatographic columns for separating magnetically labeled targets from non-magnetic entities in late 1980s while naming the technique magnetic-activated cell sorting (MACS). Since then, the positive magnetophoretic technique has been implemented in microfluidic devices, for instance, to achieve separation of two similar-sized particles based on the difference in their magnetic properties (Inglis et al. 2004). Very recently, magnetic manipulation of non-magnetic particles inside a ferrofluid has also been successfully demonstrated (Hejazian et al. 2015b). Over the past two decades, microfluidic-based magnetophoretic separation has showed a great potential for development of cost-effective and portable particle sorting technologies with some simpler systems already making their way to the market by companies such as Miltenyi Biotech and BioLegend. However, achieving multiplex sorting of magnetic and non-magnetic particles at high throughput and without the need for a sheath flow still remains a challenge in this field.

It has been reported that generation of a high-gradient magnetic field (HGMF) inside microfluidic devices and close to the stream of particles can improve the magnetic sorting performance significantly (Oberteuffer 2002). HGMF in microfluidic devices can be generated by integration of soft magnetic materials inside microchannels and their magnetization either by electromagnets or by permanent magnets. Rong et al. (2006) developed an on-chip magnetic bead sorter using six solenoid-type microinductors for sorting and transferring 8 μm magnetic particle from an input stream to a collection outlet in the device. They reported that the sorting of magnetic beads was possible only at a low flow velocity of 60 μm h^{-1}. Xia et al. (2006) demonstrated sorting of 1.6 μm magnetic particles from 2 μm non-magnetic particles at a throughput of ~10^6 particles per hour using a needle- or comb-shaped HGMF concentrator made from NiFe (80% Nickel, 20% Iron). Giudice et al. (2015) demonstrated two-particle sorting, i.e., 6 or 20 μm non-magnetic particles from 10 μm magnetic particles, dispersed in a viscoelastic solution with a separation efficiency of up to 96%. The

technique required an external buffer flow for sorting and the maximum flow rate of operation was 240 μl h^{-1}. Tsai et al. (2011) demonstrated separation of 0.5 μm magnetic particles from 1.6 μm magnetic particles using a permanent magnet in a straight microchannel; however, a sheath flow for performing separation was again required in their device. Inglis et al. (2004) embedded nickel magnetic stripes into a microfluidic channel and magnetized them using an external permanent magnet for separating two targets at a flow velocity of 240 μm s^{-1}. The particles had to be aligned with a sheath flow, and the process of fabricating the magnetic stripes in the narrow microchannel was relatively complex. Recently, we demonstrated a method for size-based fractionation of 5 μm magnetic particles from 11 μm ones in a microfluidic device (Kumar and Rezai 2016). This hybrid technique was devised based on a combination of magnetic focusing of particles against the wall of a microchannel and their hydrodynamic fractionation downstream. It required no sheath flow and could be operated at a flow velocity of 0.3 m s^{-1}, which was significantly higher than majority of above-mentioned methods.

Several attempts have been made to separate more than two particles in magnetophoretic devices to address the technological need of multiplex fractionation in handling complex mixtures such as blood and water. Adams et al. (2008) demonstrated triplex sorting and separated two magnetic particles from a non-magnetic particle, using a similar technique as reported by Inglis et al. (2004). Essentially, they fabricated two regions of magnetic strips in their microchannel for deflecting magnetic particles at different angles into two collection channels and restricted non-magnetic particles from entering into collection outlets using an excessive sheath flow. Chalmers et al. (1998) used magnetic dipole and quadrupole to separate targets based on their extent of magnetic labeling at a throughput of ~10^6 particles per hour. Pamme and Manz (2004) performed continuous triplex sorting and separated 2 and 4.5 μm magnetic particles from 6 μm non-magnetic particles using a sheath flow to focus the particles in a channel with a side-channel magnet to sort the particles at a throughput of ~720 particles per hour. All in all, current magnetophoretic-based particle sorting techniques can achieve triplex sorting at low flow rates while suffering from shortcomings such as a need for sheath flow and fabrication of delicate microstrips to achieve HGMF in the channel.

In this paper, we introduce a novel hybrid technique called Multiplex Inertio-Magnetic Fractionation (MIMF) to simultaneously fractionate up to four microparticles in water at a throughput of 10^6–10^9 particles per hour. MIMF is based on interaction between inertial and magnetic forces for achieving fourplex fractionation of microparticles in a microchannel. In comparison with our duplex method (Kumar and Rezai 2016) that was capable of fractionating

10^7 magnetic particles per hour at low flow rates (due to magnetic force dominance), MIMF can fractionate magnetic particles from each other and from closely sized non-magnetic particles (duplex to fourplex) at several orders of magnitude higher throughputs by taking advantage of inertial forces that become dominant in our device upon optimizing geometry and at desirably higher flow rates. We firstly conducted a comprehensive parametric study to investigate the effect of flow rate, channel aspect ratio and particle size on duplex MIMF to understand the behavior of particles in our device. We then used the obtained knowledge to demonstrate triplex and fourplex MIMF of magnetic and non-magnetic particles in the device at high throughputs and fractionation efficiencies. We anticipate adoption of MIMF in immunomagnetic separation applications in which multiple target biological substances such as biomolecules, cells and microorganisms need to be tagged and separated from each other and from nontargets in various types of fluids.

2 Materials and methods

2.1 Microparticles and materials

All magnetic particles used in this study were paramagnetic. Polystyrene magnetic beads referred to as 5 μm (size distribution of 4–4.9 μm) and 11 μm (size distribution of 10–13.9 μm) magnetic particles were obtained from Spherotech Inc. (IL, USA). The 35 μm polyethylene magnetic particles (size distribution of 32–38 μm) were procured from Cospheric LLC (CA, USA). The polystyrene non-magnetic particles used in this study had an average size of 15 μm (size distribution of 10–19 μm) and were obtained from Phosphorex Inc. (MA, USA). We intentionally chose to work with poly-dispersed non-magnetic particles due to two reasons. First, to use them as surrogates for a variety of nontarget non-magnetic materials (e.g., bacteria in water) in the future application of MIMF in immuno-magnetic separation of multiple magnetically tagged target analytes from nontargets and the solution. Second, to demonstrate that two closely sized particles, one magnetic (10–13.9 μm) and one non-magnetic (10–19 μm) could also be sorted in our device at high throughput and efficiency.

Silicon wafers and SU-8 2035 photoresist required for device master mold fabrication were procured from Wafer World Inc. (FL, USA) and MicroChem Corp. (MA, USA), respectively. Polydimethylsiloxane or PDMS (Sylgard 184 kit) for soft lithography-based replication of MIMF microfluidic devices was obtained from Dow Corning Corp. (MI, USA), and Tween 20 was procured from Sigma-Aldrich (MO, USA). Neodymium N42 grade cuboid magnet (length 25 mm, width 10 mm and height 2.5 mm) used for magnetic separation of particles in the MIMF device was obtained from Indigo Instruments (Waterloo, ON, Canada).

Fig. 1 The Multiplex Inertio-Magnetic Fractionation (MIMF) device is shown in (a) and schematically in (b). The device (*scale bar* 25 mm) consisted of an inertio-magnetic zone (IMZ) with a side permanent magnet and an expansion zone (EZ). The schematic representation of MIMF device conceptually shows simultaneous fractionation of four particles, i.e., three *red-colored* magnetic particles (MP) of different sizes from a *black-colored* non-magnetic particle (NMP). The NMPs inertially focus at the center of the channel, while MPs get fractionated based on interaction between inertial and magnetic forces and positioned according to their sizes in the device with smaller particles located closer to the wall (color figure online)
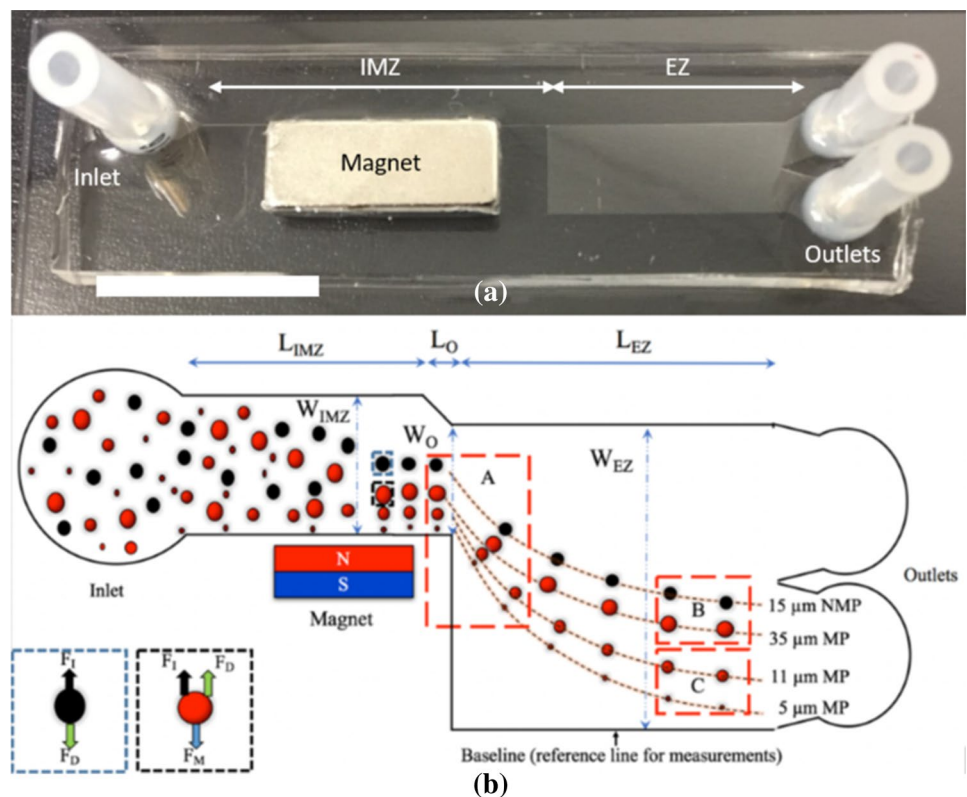
2.2 Design and fabrication of MIMF device

The device, which is presented in Fig. 1a, contained two distinct zones, i.e., the inertio-magnetic zone (IMZ) and the expansion zone (EZ) that are more clearly demonstrated in the schematic diagram of Fig. 1b (not to scale). The IMZ consisted of a $L_{IMZ} = 40$ mm and $W_{IMZ} = 90$ μm microchannel with various heights (30, 40, 50 and 60 μm) to investigate the effect of aspect ratio (AR = width/height) and hence inertial forces (F_I in Fig. 1b; Liu et al. 2015; Wang et al. 2016; Wu et al. 2016) on MIMF. The permanent magnet was positioned 0.5 and 7.5 mm away from the IMZ and EZ (edge-to-edge distance), respectively, in order to apply magnetic forces (F_M in Fig. 1b) to the magnetic particles flowing in the channel. The EZ ($L_{EZ} = 30$ mm and $W_{EZ} = 11$ mm) was simply implemented to hydrodynamically separate the focused particles and further fractionate and image them in the device, conceptually similar to the PFF method (Yamada et al. 2004; Sai et al. 2006; Vig and Kristensen 2008). The focus of this paper was to investigate the concept of Multiplex Inertio-Magnetic Fractionation of microparticles and not sorting; hence, only two outlets were implemented in this device. However, the findings can easily be used as a design guideline to add outlets at desirable locations in the channel for future sorting of particles or particle–analyte conjugates.

The device could easily be fabricated from a single layer of patterned PDMS, a glass slide and a low-cost permanent magnet. The master mold for our MIMF device was fabricated on a 4-in silicon wafer with SU-8 2035, using a standard photolithography technique (Qin et al. 2010). A magnet template was then positioned on the master mold at a location designated with alignment marks on the mold. PDMS pre-polymer in 10:1 base to crosslinking agent ratio was prepared and cast over the mold and then heat cured at 80 °C for 2 h. The cured PDMS layer was peeled off the master mold, the magnet template was removed, and the layer was bonded against the glass slide using oxygen enhanced plasma to obtain the final device. The permanent magnet was then positioned in its prefabricated location, and inlet and outlet tubes were installed in-place for operating the device. The precise location of the magnet with respect to the IMZ channel was checked under a microscope before each experiment.

2.3 Experimental procedure and data analysis

Duplex, triplex and fourplex mixtures of particles at desirable concentrations (10^4–10^8 particles per ml) in deionized water were prepared off the chip and injected into devices with various geometries using a syringe pump (Legato 110, KD Scientific, USA). The sample input flow rate was varied (1–9 ml h^{-1}) to study the effect of flow rate on MIMF performance with no need for a sheath flow in this method. Images and videos of particles distribution were captured at Regions A, B and C (Fig. 1b) of the device using a camera (GS3-U3-23S6C-C, Point Grey, BC, Canada) at a frame rate of 162 frames per second, mounted on an inverted microscope (BIM500FL, Bioimager, ON, Canada). Before performing any imaging and as a precaution, we ran the experiments for 15 min to allow the flow to stabilize in the device although fractionation was observed within 1–2 min of sample injection. The freeware ImageJ was used for analyzing the captured images of particles in the device. For quantifying the position of particles, we partitioned the image into a sequence of narrow windows of 100 μm height and used the "analyse particle" function in ImageJ for counting the number of particles in each of these windows.

3 Working principle and dominant forces

For a laminar flow in a circular microchannel, it has been found that spherical microparticles tend to focus at a distance 0.6 times the radius away from the center of the channel (Segré and Silberberg 1961). It has been shown that focusing is promoted by net inertial lift forces acting on these particles in a microchannel (Di Carlo et al. 2007; Martel and Toner 2014). It has also been reported that particles tend to focus at two central equilibrium positions when flowing in a rectangular channel with AR (=width/height) > 1 (Zhou and Papautsky 2013). The net inertial lift force acting on the particles in the direction transverse to the flow (Fig. 1b) can be expressed as (Zhou and Papautsky 2013):

$$F_I = C_L \frac{4U_f^2}{D_h^2} \rho a^4 \tag{1}$$

where C_L is the lift coefficient that can be approximated to be 0.5 (Asmolov 1999), U_f is average flow velocity (m s^{-1}), D_h is hydraulic diameter of the channel (m), ρ is density of the fluid (Kg m^{-3}) and a is the diameter of particles (m). The channel (Re$_c = \rho U_m D_h/\mu$) and particle (Re$_p =$ Re$_c(a/D_h)^2$) Reynolds numbers are used to assess the inertial focusing of particles in microchannels (Di Carlo et al. 2007). In these equations, U_m is the maximum flow velocity (m s^{-1}) and μ is the dynamic viscosity (Pa s) of the fluid. It has been highlighted in several reports that inertial forces significantly affect the focusing of microparticles in microchannels when Re$_p$ is of order 1 and greater (Xuan et al. 2010; Martel and Toner 2014). We have also adopted this criterion to explain the fractionation of microparticles in our MIMF device.

Another dominant force is the stokes drag force (F_D in Fig. 1b) that acts against the lateral motion direction of microparticles in the channel. The magnitude of stokes drag force can be expressed as (Zhou and Papautsky 2013):

$$F_D = 3\pi\mu a U_L \qquad (2)$$

where U_L is the velocity (m s^{-1}) of particles in the lateral direction. The drag force does not influence the equilibrium position of the particles; it only affects the particle displacement velocity toward the final state at which $F_D = 0$.

Finally, the force acting on a magnetic particle due to a permanent magnet such as the one used in our device can be expressed as (Adams et al. 2008):

$$F_M = \frac{4\pi}{3} M \nabla B r^3 \qquad (3)$$

where r is the radius of particle (m), M is magnetization (A m^{-1}) and ∇B is magnetic field gradient (T m^{-1}). Based on the data provided by Indigo Instruments and our approximations, magnetization was 2.7×10^6 A m^{-1}, magnetic field gradient was 10 T m^{-1}, and magnetic field magnitude inside the channel was 300 mT (enough for saturated magnetization of particles). According to magnetic particle vendors, ~10% of the particles was made of magnetite with provided magnetic susceptibility of 11.4. Magnetic moments approximated for the particles based on the information provided above were 1.8×10^{-11}, 1.9×10^{-10} and 6.1×10^{-9} for 5, 15 and 35 μm magnetic particles, respectively. We used these data to calculate the order of magnitude of magnetic forces in comparison with inertial forces in our experiments. Readers are referred to more thorough papers on magnetism in microfluidic devices for theoretical understanding of magnetic forces in microchannels (Pamme 2006; Hejazian et al. 2015a).

According to Eqs. (1)–(3), before reaching equilibrium positions, magnetic particles are under the effect of magnetic, drag and inertial lift forces as schematically shown in Fig. 1b, while non-magnetic particles are under the effect of drag and inertial lift forces only. The direction of inertial and magnetic forces shown in Fig. 1b is only applicable to particles positioned in the bottom half of the channel closer to the permanent magnet. For magnetic particles in the top half of the channel, the direction of magnetic and inertial forces will both be toward the channel center. The direction of drag forces can vary for different particles dependent on their direction of motion toward the wall (magnetic dominance) or the center (inertia dominance) of the channel. The drag force drops to zero as the particles arrive at their equilibrium states in the channel ($F_I = F_M$ and $U_L = 0$ m s^{-1}).

Multiplex particle fractionation is achievable in our MIMF device owing to interaction between magnetic, drag and inertial lift forces. Hypothetically, the device should be capable of focusing non-magnetic particles (NMP) inertially at the center of the channel if $Re_{p,NMP}$ is significantly greater than 1, while fractionating the magnetic particles (MP) across the width of the channel if $Re_{p,MP}$ does not significantly exceed unity (i.e., magnetic and inertial forces act comparatively on these particles). Upon maintaining the magnetic field gradient constant, the movement of particles inside our device would be dependent mostly on input flow rate, channel aspect ratio (or hydralic diameter) and particle sizes. Effects of these parameters have been investigated to devise a fourplex particle fractionation microdevice. Our focus was multiplex fractionation in water so the effects of fluid properties were not studied in this paper.

4 Results and discussions

In this section, we first parametrically investigated the effects of flow rate, channel aspect ratio and particle size on movement of magnetic and non-magnetic particles under positive magnetophoresis conditions in the MIMF device. We favored investigating the effect of flow rate (over flow velocity) because maintaining the flow rate at a high level is an important and pressing need for the application of sorting devices in many fields such as water and body fluid monitoring and detection. The outcomes of parametric studies were then used to demonstrate multiplex MIMF of particles simultaneously in our device (Fig. 1).

4.1 Duplex MIMF and parametric studies

As described in Sect. 3, a mixture of magnetic and non-magnetic particles injected into our device would tend to get inertially focused in the center of the channel in the absence of any magnetic force. However, only magnetic particles will be attracted toward the wall of the channel and get separated from the stream of non-magnetic particles upon positioning a magnet in the device. This scheme of separation would be feasible given that there is a sufficient inertial force acting on both particles, while the magnetic force acting on magnetic particles is strong enough to overcome the inertial forces. Hence, it is important to optimize the operating conditions of the device so as to achieve coexistence of magnetic and inertial forces of appropriate magnitudes but opposite directions. These forces are dependent on parameters such as flow rate, channel aspect ratio and particle sizes (Eqs. 1–3) under constant magnetic field conditions. A series of experiments were performed to ascertain the effect of these parameters on distribution of particles in our device. The findings were applied to discern optimum conditions for achieving two-particle fractionation, with size similarity, in the MIMF device.
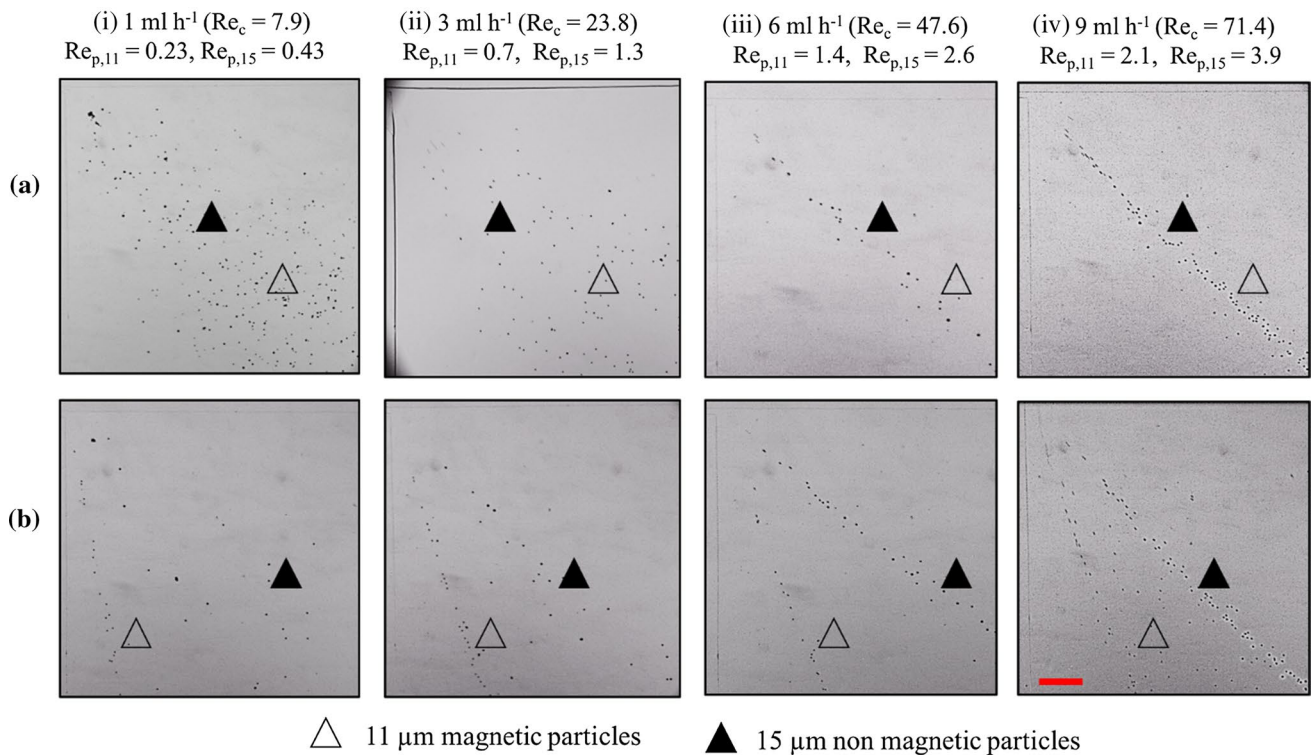
(i) 1 ml h^{-1} (Re$_c$ = 7.9)
Re$_{p,11}$ = 0.23, Re$_{p,15}$ = 0.43

(ii) 3 ml h^{-1} (Re$_c$ = 23.8)
Re$_{p,11}$ = 0.7, Re$_{p,15}$ = 1.3

(iii) 6 ml h^{-1} (Re$_c$ = 47.6)
Re$_{p,11}$ = 1.4, Re$_{p,15}$ = 2.6

(iv) 9 ml h^{-1} (Re$_c$ = 71.4)
Re$_{p,11}$ = 2.1, Re$_{p,15}$ = 3.9

(a)

(b)

△ 11 μm magnetic particles   ▲ 15 μm non magnetic particles

Fig. 2 Experimental observations of the effect of flow rate (1–9 ml h^{-1}) on behavior of 11 μm magnetic and 15 μm non-magnetic particles in Region A of the MIMF device with AR of 1.8. **a** (i–iv) show the results without any magnet in the setup, while **b** (i–iv) demonstrate the results at identical conditions but with presence of the permanent magnet in the setup. The flow direction was from *left* to *right* in all images, and the *scale bar* corresponds to 250 μm

4.1.1 Effect of flow rate on duplex MIMF

Experiments were performed with a mixture of 11 μm (10–13.9 μm) magnetic and 15 μm (10–19 μm) non-magnetic particles in the device with AR of 1.8 as discussed in Materials and Methods section. There were a total of approximately 10^6 particles per ml of sample used in this study. We varied the input flow rate from 1 to 9 ml h^{-1} and captured distribution of particles in the expansion region of the device (Regions A, B and C in Fig. 1). The experiments were firstly performed without any magnet to gauge the distribution of particles with respect to inertial and drag forces generated in the device as shown in Fig. 2a (i–iv). We observed that both particles were randomly distributed across the width of the channel at lower flow rates [<6 ml h^{-1}, when the corresponding Re$_p$ was 0.23–1.3 for both particles, Fig. 2a (i, ii)] which confirmed the absence of significant inertial forces in the device to focus the particles. However, particles started getting focused in the center of the channel at higher flow rates (>6 ml h^{-1}) as observed in Fig. 2a (iii, iv). In these cases, the inertial forces grew in magnitude and were able to dominate the distribution of particles as Re$_p$ became greater than 1.4 for 11 μm magnetic particles and 2.6 for 15 μm non-magnetic particles.

The above experiments were repeated under same operating conditions with a magnet in the setup. Observations of particles distribution is presented in Fig. 2b (i–iv). At all flow rates under 9 ml h^{-1}, the magnetic particles were magnetically focused closer to the channel wall of the expansion region (i.e., inertia less significant, Re$_{p,11}$ < 1.4). The non-magnetic particles were found dispersed in the channel at flow rates less than 6 ml h^{-1} as described above; however, they got strongly focused in the center at flow rates of more than 6 ml h^{-1} (Re$_{p,15}$ = 2.6 and higher). At a flow rate of 6 ml h^{-1}, it was found that both magnetic and non-magnetic particles were focused in the device and completely separated from each other. Interestingly, at the flow rate of 9 ml h^{-1} (Re$_c$ = 71.4), we observed that 11 μm magnetic particles were slightly defocused in the expansion channel, while the 15 μm non-magnetic particles were still strongly focused. Accordingly, no separation was possible at this flow rate as the inertial forces started to become stronger (Re$_{p,11}$ = 2.1) than the magnetic forces and push the magnetic particles toward the center of the channel. Hence, we concluded that particle manipulation was governed by magnetic focusing at flow rates <6 ml h^{-1} and by inertial focusing at flow rates > 6 ml h^{-1} in this device (AR = 1.8). In terms of particle Reynolds number, fractionation was
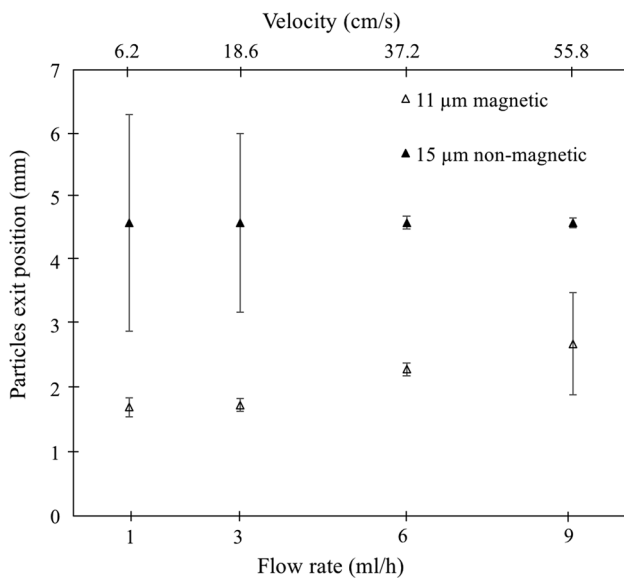
Fig. 3 Quantification of exit position (mean and standard deviation) of 11 μm magnetic and 15 μm non-magnetic particles in the MIMF device with AR of 1.8 when experiments were performed with a magnet at various flow rates. The exit positions were measured with respect to the baseline of the device

stronger when Re_p was close to one for 11 μm magnetic and more than two for 15 μm non-magnetic particles [Fig. 2b (iii)].

We also measured the exit position of particles at Regions B and C of the device with respect to the expansion channel baseline, using the method detailed in Materials and Methods section. Figure 3 shows the mean position and distribution of both 11 μm magnetic and 15 μm non-magnetic particles when experiments were performed with a magnet in the setup corresponding to observed distributions in Fig. 2b (i–iv). At low flow rates of 1 and 3 ml h^{-1}, the non-magnetic particles were dispersed over the regions 4.60 ± 1.70 and 4.60 ± 1.40 mm away from the baseline, respectively. However, the 11 μm magnetic particles were focused over the regions 1.71 ± 0.15 and 1.74 ± 0.10 mm away from the baseline at the low flow rates of 1 and 3 ml h^{-1}, respectively. At 6 ml h^{-1}, the 11 μm magnetic particles were still focused; however, they were found to be slightly shifted toward the center of the channel at 2.30 ± 0.10 mm away from the baseline. The non-magnetic particles were also focused in the region 4.60 ± 0.12 mm away from the baseline at 6 ml h^{-1} due to dominance of inertial forces illustrated in Fig. 2. At 9 ml h^{-1}, the 11 μm magnetic particles were slightly defocused due to excess inertial forces and distributed over region 2.70 ± 0.80 mm away from the baseline, while 15 μm non-magnetic particles were still focused at 4.60 ± 0.10 mm away from the baseline. It is worth mentioning that a series of experiments performed with one type of particle at a time (data not

shown) resulted in the same lateral distribution of particles shown in Fig. 3, verifying that interaction of different particles did not have a significant effect on our results at the particle concentration levels used in these studies.

Essentially, inertial forces could be used as a means to differentiate non-magnetic particles from magnetic particles in a sheathless fashion and without any need for HGMF elements like magnetic comb, needle or stripes (Inglis et al. 2004; Xia et al. 2006; Adams et al. 2008). However, we noticed that inertial forces grow in magnitude with increase in flow rate and eventually interfered with magnetic focusing of magnetic particles. Hence, it is required that the device performance be characterized to achieve an optimal flow rate where inertial and magnetic forces are of appropriate magnitudes. The intermediate flow rate regime of 6 ml h^{-1} ($Re_c = 47.6$, Figs. 2, 3) is the optimal choice for achieving fractionation of magnetic particles from non-magnetic particles in the device with AR = 1.8, as there is coexistence of inertial and magnetic focusing under this condition.

4.1.2 Effect of channel aspect ratio on duplex MIMF

The ratio of particle size to characteristic length of the channel significantly affects the magnitude of inertial focusing forces exerted onto particles (Eq. 1). In this section, the effect of AR on the distribution of particles in the expansion region of the device (Regions A, B and C shown in Fig. 1) was investigated. Aspect ratios of 1.8, 2.25 and 3 were tested by fabricating devices with heights of 50, 40 and 30 μm, respectively. The experiments were performed with a mixture of 11 μm magnetic and 15 μm non-magnetic particles in the device at flow rates of 1, 3, 6 and 9 ml h^{-1} with a magnet in the setup. There were a total of approximately 10^6 particles per ml of sample used in this study. The results of observed distribution of particles in Region A of the device are shown in Fig. 4.

As shown in Fig. 4, at a flow rate of 1 ml h^{-1}, the change in AR from 1.8 to 3 led to enhancement of inertial focusing of non-magnetic particles owing to increase in particle Reynolds number ($Re_{p,15}$) from 0.43 to 1. We found that 15 μm non-magnetic particles were focused in the center of the device with AR of 3; however, they were found to be randomly distributed in the device with AR of 1.8. The 11 μm magnetic particles were found to be focused magnetically close to the sidewall in all three devices at this low flow rate. $Re_{p,11}$ increased from 0.23 in device with AR = 1.8 to 0.6 when AR = 3, at which inertial focusing is not very strong allowing the 11 μm particles to be under the dominant effect of magnetic forces. At a flow rate of 3 ml h^{-1}, it was observed that 15 μm non-magnetic particles were slightly defocused in the device with AR of 1.8 ($Re_{p,15} = 1.3$), but focused in the other two devices
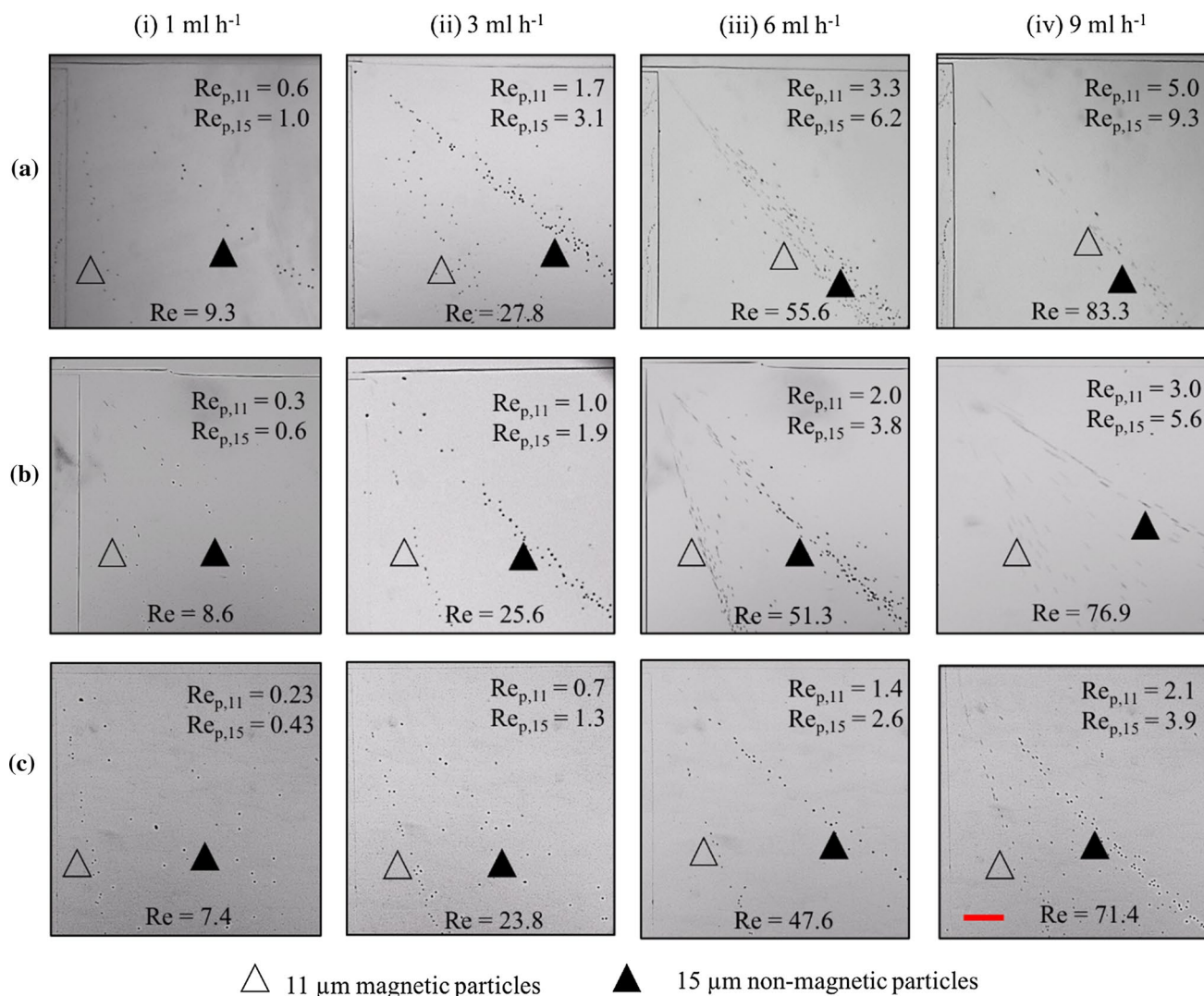
Fig. 4 Experimental observations of the effect of channel aspect ratio (AR = width/height) on behavior of 11 μm magnetic and 15 μm non-magnetic particles in Region A of the MIMF device at various flow rates (columns). Rows **a**, **b** and **c** correspond to experiments performed with device ARs of 3, 2.25 and 1.8, respectively. The flow direction was from *left* to *right* in all images, and the *scale bar* corresponds to 250 μm

($Re_{p,15}$ = 1.9 for AR = 2.25 and $Re_{p,15}$ = 3.1 for AR = 3). The 11 μm magnetic particles, however, were found to be slightly defocused from the wall (due to inertia) in the device with AR of 3 ($Re_{p,11}$ = 1.7) but still well-focused magnetically at the wall in the devices with AR of 2.25 ($Re_{p,11}$ = 1) and 1.8 ($Re_{p,11}$ = 0.7) at a flow rate of 3 ml h^{-1}. It is worth noting that fractionation of magnetic particles from non-magnetic particles in the device with AR of 3 was not possible at any flow rate higher than 3 ml h^{-1}. At a flow rate of 6 ml h^{-1}, we found that both magnetic and non-magnetic particles were separately focused in the device with AR of 2.25 ($Re_{p,11}$ = 2.0 and $Re_{p,15}$ = 3.8) and 1.8 ($Re_{p,11}$ = 1.4 and $Re_{p,15}$ = 2.6) with some inertial defocusing of magnetic particles in the device with AR of 2.25 due to the high $Re_{p,11}$ = 2.0. Fractionation of magnetic particles

from non-magnetic particles was not possible efficiently in any of the devices at a flow rate of 9 ml h^{-1} ($Re_{p,11}$ = 5.0, $Re_{p,15}$ = 9.3 for AR = 3; $Re_{p,11}$ = 3.0, $Re_{p,15}$ = 5.6 for AR = 2.25; and $Re_{p,11}$ = 2.1, $Re_{p,15}$ = 3.9 for AR = 1.8) because magnetic particles were either inertially focused and mixed with non-magnetic ones in the center (AR = 3) or dispersed in the channel due to strength of inertial forces over magnetic forces (AR = 1.8 and 2.25).

The results in Fig. 4 fully support our claim of the need for interaction between comparable inertial and magnetic forces to achieve efficient fractionation in our device. Overall, we observed that with the decrease in AR (i.e., increase in channel height), inertial forces acting on both particles decreased at a given flow rate (due to drop in the axial velocity), which in turn allowed the magnetic forces
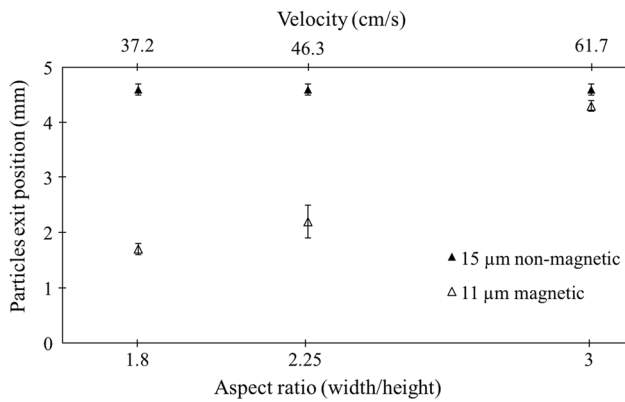
Fig. 5 Quantification of exit position (mean and standard deviation) of 11 μm magnetic and 15 μm non-magnetic particles in MIMF devices with ARs of 1.8, 2.25 and 3, at a flow rate of 6 ml h^{-1}. The exit positions were measured with respect to the baseline of the device

to become comparatively dominant on 11 μm magnetic particles to pull them away from the stream of 15 μm non-magnetic particles. Accordingly, distinct separation of the two particle streams could be obtained at higher flow rates when AR of the MIMF device was reduced. The observation pertaining to insufficient separation in the device with AR of 3 at any flow rate greater than 3 ml h^{-1} (Re$_{p,11}$ > 3.3 and Re$_{p,15}$ > 6.2) can be attributed to dominance of inertial forces at high flow velocities over magnetic forces as explained by Eqs. 1 and 3.

Positional distribution of 11 μm magnetic and 15 μm non-magnetic particles at 6 ml h^{-1} flow rate (Fig. 4iii) was quantified in Regions B and C of the device (Fig. 1), assuming baseline as the reference and results are presented in Fig. 5. It was found that 15 μm non-magnetic particles were concentrated in the region 4.60 ± 0.10 mm away from the baseline in all three devices. However, the 11 μm magnetic particles were concentrated at 1.70 ± 0.10, 2.20 ± 0.3 and 4.30 ± 0.1 mm away from the baseline in the devices with AR of 1.8, 2.25 and 3, respectively. This quantitative result also demonstrates the shifting of magnetic particles from the sidewall toward the center of the channel as the AR is increased, confirming that inertial forces become more dominant on all particles as the height of the channel decreases from 50 μm to 30 μm.

In a nutshell, the investigation of aspect ratio of devices with the objective of keeping the flow rate high led to two important conclusions. Firstly, the distribution of particles greatly varies with change in AR of the device, and hence, the device design must be done carefully to achieve the desired results. Especially, the separation scheme is more feasible when the particle Reynolds number for 11 μm magnetic particle (Re$_{p,11}$)

is closer to 1. Secondly, Fig. 4 clearly shows that it is possible to improve the throughput of fractionation from 1 to 6 ml h^{-1} just by adjusting the AR from 3 to 1.8. This better understanding of behavior of particles with respect to AR of the channel enabled development of MIMF devices with throughputs higher than 6 ml h^{-1} for fractionation of two to four particles in the rest of the paper.

4.1.3 Effect of size of magnetic particles on duplex MIMF

The magnitude of inertial forces, as shown in Eq. 1, is strongly affected by the size of particles (Di Carlo et al. 2007; Zhou and Papautsky 2013). Herein, we performed the duplex fractionation experiments with magnetic particles of diameter 5, 11 or 35 μm mixed one at a time with 15 μm non-magnetic particles to elucidate the effect of size on the dynamic competition between inertial and magnetic forces. We chose these sizes to ensure that the MIMF principle can be applied for fractionating a wide range of targets from a mixture. The experiments in previous section indicated that the device throughput can be improved by decreasing the AR of the channel. Hence, we chose to perform this set of experiments in a MIMF device with AR of 1.5 to achieve fractionation at a higher flow rate of 9 ml h^{-1} that was not achievable with the previous devices. Figure 6 shows the distribution of the above-mentioned pairs of particles after fractionation in the channel at Region C of the device.

In the experiments conducted with a mixture of 5 μm magnetic and 15 μm non-magnetic particles, it was found that non-magnetic particles were focused close to the center of the channel, 4.70 ± 0.12 mm away from the baseline, because of dominant inertial forces at 9 ml h^{-1}
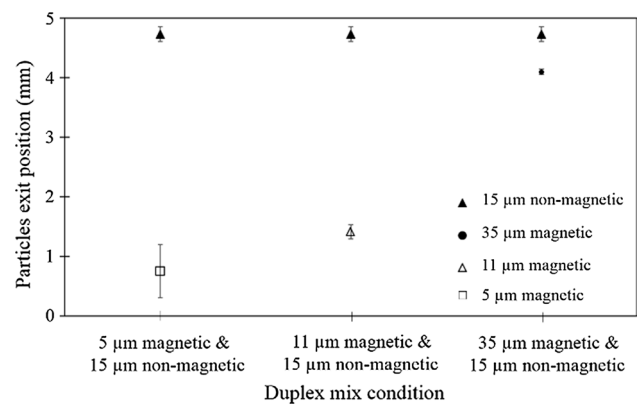

Fig. 6 Quantification of exit position (mean and standard deviation) of various sizes (5, 11 or 35 μm) of magnetic particles sorted one at a time from 15 μm non-magnetic particles in a duplex MIMF devices with AR of 1.5 at a flow rate of 9 ml h^{-1}. The exit positions were measured with respect to the baseline of the device

flow rate ($Re_{p,15} = 2.9$). The 5 µm magnetic particles were found to be distributed at 0.64 ± 0.34 mm and completely fractionated from the non-magnetic particles ($Re_{p,5} = 0.3$, hence no inertial focusing). The experiments were performed at a concentration of approximately 10^8 particles per ml of water (mixture of ~10^8 magnetic and ~10^5 non-magnetic particles per ml), which resulted in an unprecedented high throughput of 10^9 particles per hour.

In the experiments performed with a mixture of 11 µm magnetic and 15 µm non-magnetic particles, the magnetic particles ($Re_{p,11} = 1.6$, weaker inertial forces overpowered by magnetic forces) were magnetically focused in the region around 1.41 ± 0.12 mm away from the baseline, while non-magnetic particles were found inertially focused close to the center as before. This fractionation study was performed at a throughput of 10^7 particles per hour as the concentration of particles used for experiments was about 10^6 particles per ml of water (mixture of ~10^6 per ml magnetic and ~10^5 per ml non-magnetic particles).

When 35 µm magnetic particles were tested in mixture with 15 µm non-magnetic particles, they were found distributed over the region 4.10 ± 0.04 mm away from the baseline ($Re_{p,35} = 15.8$). Since $Re_{p,35}$ was much greater than 1, these particles experienced more significant inertial forces than the 5 and 11 µm magnetic particles in previous experiments and were focused closer to the center of the channel. However, magnetic forces were still able to pull them away from the stream of non-magnetic particles focused purely by inertia at the center of the channel. The throughput of these experiments was about 10^6 particles per hour as the study was conducted at a concentration of

about 10^5 particles per ml (mixture of ~10^4 per ml magnetic and ~10^5 per ml non-magnetic particles).

We observed that there was a complete fractionation of each type of magnetic particles from non-magnetic particles in all three experiments described above. Moreover, quantification of positions of particles in the device led to a finding that the larger the magnetic particles were, the closer they became to the stream of 15 µm non-magnetic particles in the center of the channel. This can be explained by the magnitude of inertial forces that increases more rapidly with particle diameter (4th power dependence in Eq. 1) as compared to magnetic forces (third power dependence in Eq. 3). Accordingly, interaction between magnetic and inertial forces can easily be used as a scheme to achieve multiplex particle fractionation with the MIMF method. This has been pursued in the next two sections of this paper.

4.2 Triplex MIMF of magnetic particles

In this section, we investigated simultaneous fractionation of three magnetic particles of sizes 5, 11 and 35 µm with MIMF. As we observed in the previous section, cumulative effect of magnetic and inertial forces leads to size-dependent ordering of magnetic particles in the device, hence offering a scheme to perform multi-particle fractionation in an inertio-magnetic device. Experiments were performed in a MIMF device with AR of 1.5 at a flow rate of 9 ml h^{-1}. This study was conducted at a total concentration of approximately 10^6 particles per ml. Particle distribution images were captured at Region A of the device with and
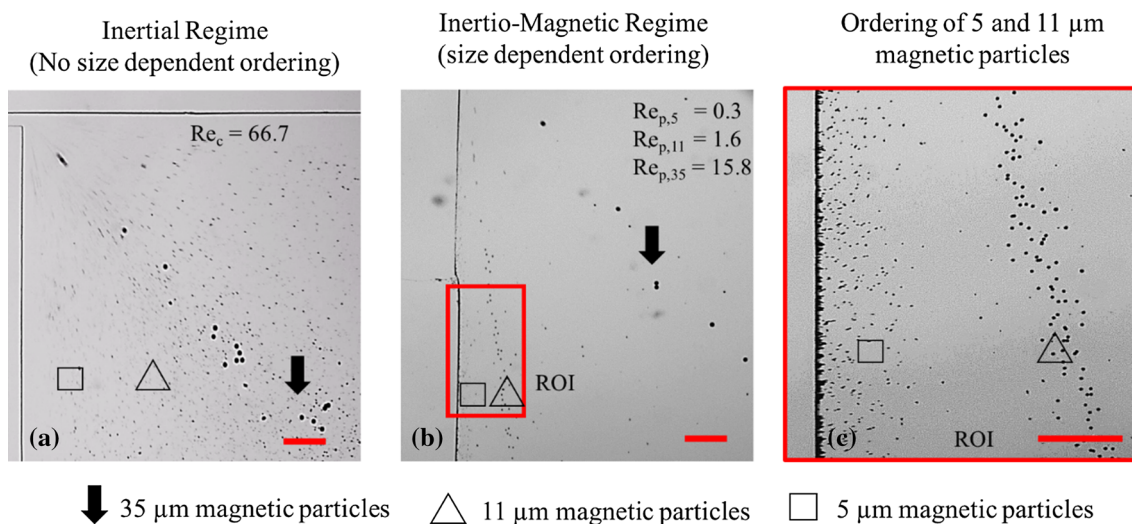

Fig. 7 Experimental observations (at Region A of the device) showing separation of 5, 11 and 35 µm magnetic particles in a MIMF device with AR = 1.5 at 9 ml h^{-1} flow rate. Distribution of all three particles is demonstrated (**a**) without any magnet and (**b–c**) with a magnet in the setup. The magnified view of 5 and 11 µm magnetic particles corresponding to the region of interest (ROI) in (**b**) is shown in (**c**). The flow direction was from *left* to *right* in all images, and *scale bars* correspond to 250 µm

without the magnet in the setup, and results are presented in Fig. 7.

Firstly, a mixture of all three particles was injected into device and their distribution was monitored in Region A without any magnet in the setup. Figure 7a shows that all particles were randomly distributed in the device in the absence of any magnetic force. We observed that 35 μm magnetic particles were focused in the center of the channel, indicating the presence of a significant inertial force on these particles ($\text{Re}_{p,35}$ = 15.8). However, it was difficult to discern the distribution of 5 and 11 μm magnetic particles distinguishably in this condition ($\text{Re}_{p,5}$ = 0.3 and $\text{Re}_{p,11}$ = 1.6). Then, we performed the same experiment involving all three particles but with a magnet in the setup and the particle distribution results are presented in Fig. 7b, c. It was found that 35 μm magnetic particles were still focused very close to the center of the channel, indicating that there was a dominance of inertial forces on these particles as discussed in the previous section and Fig. 6. Inertial forces overpowered the magnetic forces on 35 μm magnetic particles and did not allow them to be attracted much toward the magnet in the device. On the other hand, we found that 5 and 11 μm magnetic particles were more strongly attracted by the magnet and were focused much closer to the wall of the channel as compared to 35 μm magnetic particles. The streams of 5 and 11 μm magnetic particles were not clearly visible in Fig. 7b, and hence, we captured their distribution at a higher magnification as

shown in Fig. 7c. These particles were found to be completely separated from each other, and as expected, the 5 μm magnetic particles were closer to the wall than 11 μm magnetic particles. Accordingly, we experimentally verified that the smaller the magnetic particles, the closer their positions were to the wall in a MIMF setup. We emphasize that existence of one type of force in the device will either lead to no fractionation at all (with inertial forces only) or potentially fractionation at a significantly lower throughput and efficiency (with magnetic forces only) based on our previously reported method (Kumar and Rezai 2016). As demonstrated in this section, it is the proper design of the device geometries and the coexistence of inertial and magnetic forces at high flow rates that led to accomplishment of triplex fractionation at high throughputs with the MIMF method.

4.3 Fourplex MIMF of magnetic and non-magnetic particles

In immunomagnetic separation, a number of target analytes are usually needed to be magnetically tagged and separated from each other as well as other nontarget analytes. Here, we used the MIMF technique to achieve fractionation of three magnetic particles from non-magnetic particles of various sizes as surrogates for nontargets. The experiments were performed with mixtures of 5, 11 and 35 μm magnetic and 10–19 μm (called 15 μm) non-magnetic particles
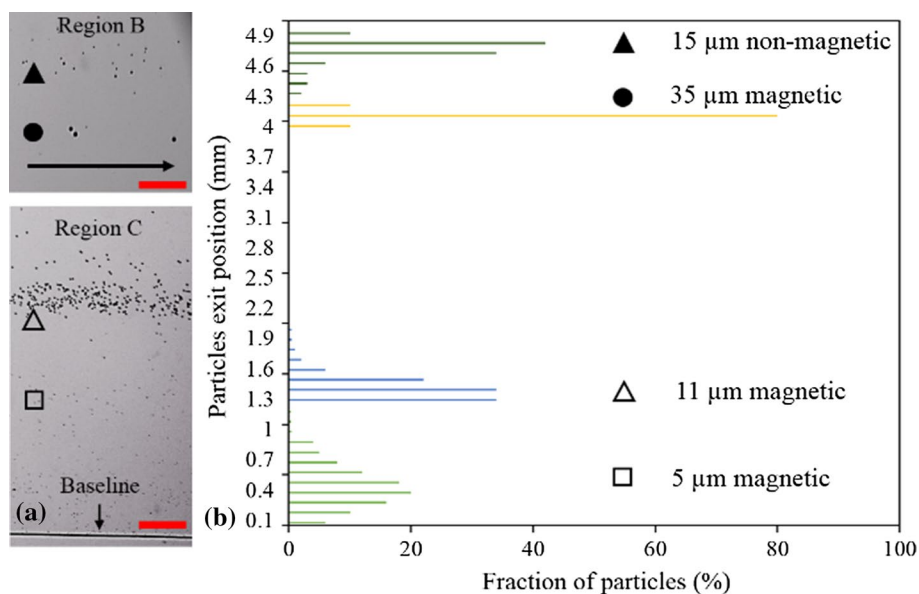

Fig. 8 Fourplex MIMF of magnetic and non-magnetic particles. **a** Experimental observations (at Regions B and C of the device) of simultaneous fractionation of four particles (5, 11 and 35 μm magnetic particles and 15 μm non-magnetic particles) in a MIMF device with AR = 1.5 at 9 ml h^{-1} flow rate. Due to limited field of view of our microscope, we captured the images of Regions B and C separately, to exhibit fractionation of all four particles in the device. The flow direction was from *left* to *right* in both images, and *scale bar* corresponds to 250 μm. **b** Quantification of exit positions and fractions of 5, 11 and 35 μm magnetic particles and 15 μm non-magnetic particles sorted in the MIMF device. The exit positions were measured with respect to the baseline of the device

in water at a total concentration of about 10^6 particles per ml. The samples were injected into the MIMF device with AR of 1.5 at a flow rate of 9 ml h^{-1} (Re$_p$ = 0.3, 1.6 and 15.8 for 5, 11 and 35 μm magnetic particles, respectively, and Re$_p$ = 2.9 for non-magnetic particles), and images were captured at Regions B and C of the device (Fig. 8a) for quantifying particles' exit positions with respect to the expansion region baseline (Fig. 8b). We could not capture the entire spectrum of four fractionated particles in one frame at the downstream region of the device due to the limited field of view of our microscope, as particle bands were distributed over a distance of about 5 mm across the width of the channel. Hence, we captured the position of 15 μm non-magnetic and 35 μm magnetic particles in one frame at Region B of the device closer to the center and 5 and 11 μm magnetic particles in the other frame at Region C closer to the wall.

As expected, the 15 μm non-magnetic particles were inertially focused in the center and the 35 μm magnetic particles were found close to the stream of non-magnetic particles as they were strongly under the effect of inertial forces owing to their large sizes (see previous section). Magnetic forces dominated the focusing of 5 and 11 μm magnetic particles in Region C of the device, and they were both focused closer to the wall and arranged in a sequence similar to what was observed in the triplex MIMF (i.e., smaller particles closer to the wall due to less dominant inertial forces).

Further, we quantified the distributed positions of all particles with respect to the baseline in the device (Fig. 8b), using the method described before. The 15 μm non-magnetic particles were found concentrated in the region 4.70 ± 0.12 mm away from the baseline, and 35 μm magnetic particles were focused at 4.10 ± 0.04 mm. Both of these particles were under the dominant influence of inertial focusing forces, while magnetic forces separated the magnetic particles from the non-magnetic ones. The 11 μm magnetic particles were found closer to the wall and at 1.41 ± 0.12 mm away from the baseline, while 5 μm magnetic particles were found at 0.49 ± 0.22 mm, both under the dominant effect of magnetic forces while taking advantage of inertial competing forces to get separated from each other.

The position of fractionated particles has been provided as guideline here, and these particles can easily be collected separately by implementing outlets based on the calculated exit positions of these particles presented in Fig. 8. This was outside the scope of this research and will be pursued in the future for sorting of microorganisms based on the MIMF method. It should be highlighted that, for this particular MIMF design and flow rate condition, the largest magnetic particles that could be separated from non-magnetic particles in our device

were 35 μm in diameter. Any further increase in the size of magnetic particles could led to their mixing with the non-magnetic particles. Moreover, another magnetic particle with an approximate size of 20 μm may also be added for further multiplexing purposes. Similarly, particles repelled by the magnetic field can also be explored in the future for sorting in the MIMF device. We anticipate that they will occupy equilibrium positions in the top half of the channel. It should be noted that although the MIMF method is strong in multiplex fractionation based on inertio–magnetic forces, it has its own limitations in terms of the size of particles that can be handled with this device. We anticipate that our proof-of-principle results will pave the way for further investigation of this hybrid method to develop custom-designed MIMF devices based on end user needs with respect to number and size of particles, throughput and fractionation efficiency.

5 Conclusions

We have presented a novel MIMF method for fractionation of up to four magnetic and non-magnetic microparticles in an inertio-magnetic microfluidic device, which addresses several drawbacks of currently available magnetic fractionation methods such as low throughput, requirement of sheath flow, inability to fractionate multiple targets simultaneously and complicacies in fabricating special HGMF elements such as magnetic combs, stripes or needles. We have shown that magnetic forces interact with inertial forces synergistically in a straight microchannel to exhibit strong size-dependent ordering of magnetic and non-magnetic particles, hence paving the way for their fractionation at a downstream hydrodynamic expansion section. We showed that fractionation of similar-sized magnetic and non-magnetic particles in the MIMF device could be achieved efficiently at a throughput as high as 10^9 particles per hour. We identified several dominant factors governing the behavior of particles in the device and conducted experiments to elucidate their effects on fractionation performance. Further, the insights gained from these parametric studies were applied to achieve simultaneous fractionation of four particles (5, 11 and 35 μm magnetic and 15 μm non-magnetic particles) for the first time in a straight microfluidic device using inertial focusing and positive magnetophoresis. The technique is also applicable to sorting of particles in ferrofluids using negative magnetophoresis simply by positioning the permanent magnet at the opposite side of the IMZ. We envision that the MIMF technique would enable easy handling of complex and dense mixtures of particles in a wide variety of applications. The technique has

a great potential for use in affinity-based immunomagnetic tagging, extraction and sorting of multiple cells and microorganisms in body fluids and water.

References

Adams JD, Kim U, Soh HT (2008) Multitarget magnetic activated cell sorter. Proc Natl Acad Sci U S A 105:18165–18170. doi:10.1073/pnas.0809795105

Andersson H, van den Berg A (2003) Microfluidic devices for cellomics: a review. Sens Actuators B Chem 92:315–325. doi:10.1016/S0925-4005(03)00266-1

Asmolov ES (1999) The inertial lift on a spherical particle in a plane Poiseuille flow at large channel Reynolds number. J Fluid Mech 381:63–87. doi:10.1017/S0022112098003474

Bhagat AAS, Kuntaegowdanahalli SS, Kaval N et al (2010) Inertial microfluidics for sheath-less high-throughput flow cytometry. Biomed Microdevices 12:187–195. doi:10.1007/s10544-009-9374-9

Chalmers JJ, Zborowski M, Sun L, Moore L (1998) Flow through, immunomagnetic cell separation. Biotechnol Prog 14:141–148. doi:10.1021/bp970140l

Del Giudice F, Madadi H, Villone MM et al (2015) Magnetophoresis "meets" viscoelasticity: deterministic separation of magnetic particles in a modular microfluidic device. Lab Chip 15:1912–1922. doi:10.1039/C5LC00106D

Di Carlo D, Irimia D, Tompkins RG, Toner M (2007) Continuous inertial focusing, ordering, and separation of particles in microchannels. Proc Natl Acad Sci U S A 104:18892–18897. doi:10.1073/pnas.0704958104

Hejazian M, Li W, Nguyen N-T et al (2015a) Lab on a chip for continuous-flow magnetic cell separation. Lab Chip 15:959–970. doi:10.1039/C4LC01422G

Hejazian M, Nguyen N-T, Nguyen N-T et al (2015b) Negative magnetophoresis in diluted ferrofluid flow. Lab Chip 15:2998–3005. doi:10.1039/C5LC00427F

Huang LR, Cox EC, Austin RH, Sturm JC (2004) Continuous particle separation through deterministic lateral displacement. Science 304:987–990

Inglis DW, Riehn R, Austin RH, Sturm JC (2004) Continuous microfluidic immunomagnetic cell separation. Appl Phys Lett 85:5093–5095. doi:10.1063/1.1823015

Julius MH, Masuda T, Herzenberg LA (1972) Demonstration that antigen-binding cells are precursors of antibody-producing cells after purification with a fluorescence-activated cell sorter. Proc Natl Acad Sci U S A 69:1934–1938

Kumar V, Rezai P (2016) Sheathless and high throughput sorting of paramagnetic microparticles in a magneto-hydrodynamic microfluidic device, IEEE EMBC 2016, Orlando (in press)

Lim CT, Zhang Y (2007) Bead-based microfluidic immunoassays: the next generation. Biosens Bioelectron 22:1197–1204. doi:10.1016/j.bios.2006.06.005

Liu C, Hu G, Jiang X, Sun J (2015) Inertial focusing of spherical particles in rectangular microchannels over a wide range of Reynolds numbers. Lab Chip 15:1168–1177. doi:10.1039/C4LC01216J

Martel JM, Toner M (2014) Inertial focusing in microfluidics. Annu Rev Biomed Eng 16:371–396. doi:10.1146/annurev-bioeng-121813-120704

Miltenyi S, Muller W, Weichel W, Radbruch A (1990) High gradient magnetic cell separation with MACS. Cytometry 11:231–238. doi:10.1002/cyto.990110203

Oberteuffer J (2002) High gradient magnetic separation. IEEE Trans Magn 12:967–970

Ozkumur E, Shah AM, Ciciliano JC et al (2013) Inertial focusing for tumor antigen-dependent and—independent sorting of rare circulating tumor cells. Sci Transl Med 5:1–20. doi:10.1126/scitranslmed.3005616.Inertial

Pamme N (2006) Magnetism and microfluidics. Lab Chip 6:24–38. doi:10.1039/b513005k

Pamme N, Manz A (2004) On-chip free-flow magnetophoresis: continuous flow separation of magnetic particles and agglomerates. Anal Chem 76:7250–7256. doi:10.1021/ac049183o

Qin D, Xia Y, Whitesides GM (2010) Soft lithography for micro- and nanoscale patterning. Nat Protoc 5:491–502. doi:10.1038/nprot.2009.234

Rong R, Choi J-W, Ahn CH (2006) An on-chip magnetic bead separator for biocell sorting. J Micromech Microeng 16:2783–2790. doi:10.1088/0960-1317/16/12/035

Sai Y, Yamada M, Yasuda M, Seki M (2006) Continuous separation of particles using a microfluidic device equipped with flow rate control valves. J Chromatogr A 1127:214–220. doi:10.1016/j.chroma.2006.05.020

Saliba A-E, Saias L, Psychari E et al (2010) Microfluidic sorting and multimodal typing of cancer cells in self-assembled magnetic arrays. Proc Natl Acad Sci U S A 107:14524–14529. doi:10.1073/pnas.1001515107

Sarkar A, Hou HW, Mahan AE et al (2016) Multiplexed affinity-based separation of proteins and cells using inertial microfluidics. Sci Rep 6:23589. doi:10.1038/srep23589

Segré G, Silberberg A (1961) Radial particle displacements in poiseuille flow of suspensions. Nature 189:209–210. doi:10.1038/189209a0

Tsai SSH, Griffiths IM, Stone HA (2011) Microfluidic immunomagnetic multi-target sorting–a model for controlling deflection of paramagnetic beads. Lab Chip 11:2577–2582. doi:10.1039/c1lc20153k

Vig AL, Kristensen A (2008) Separation enhancement in pinched flow fractionation. Appl Phys Lett 93:3–6. doi:10.1063/1.3028652

Wang X, Liedert C, Liedert R, Papautsky I (2016) A disposable, roll-to-roll hot-embossed inertial microfluidic device for size-based sorting of microbeads and cells. Lab Chip 16:1821–1830. doi:10.1039/C6LC00215C

Wu Z, Chen Y, Wang M, Chung AJ (2016) Continuous inertial microparticle and blood cell separation in straight channels with local microstructures. Lab Chip 16:532–542. doi:10.1039/C5LC01435B

Xia N, Hunt TP, Mayers BT et al (2006) Combined microfluidic-micromagnetic separation of living cells in continuous flow. Biomed Microdevices 8:299–308. doi:10.1007/s10544-006-0033-0

Xuan X, Zhu J, Church C (2010) Particle focusing in microfluidic devices. Microfluid Nanofluid 9:1–16. doi:10.1007/s10404-010-0602-7

Yamada M, Nakashima M, Seki M (2004) Pinched flow fractionation: continuous size separation of particles utilizing a laminar flow profile in a pinched microchannel. Anal Chem 76:5465–5471. doi:10.1021/ac049863r

Yilmaz S, Singh AK (2012) Single cell genome sequencing. Curr Opin Biotechnol 23:437–443. doi:10.1016/j.copbio.2011.11.018

Zhou J, Papautsky I (2013) Fundamentals of inertial focusing in microchannels. Lab Chip 13:1121–1132. doi:10.1039/c2lc41248a

Zhu G-P, Hejiazan M, Huang X, Nguyen N-T (2014) Magnetophoresis of diamagnetic microparticles in a weak magnetic field. Lab Chip 14:4609–4615. doi:10.1039/C4LC00885E